Stacking-velocity tomography with borehole constraints for tilted TI media

Xiaoxiang Wang and Ilya Tsvankin, Center for Wave Phenomena, Colorado School of Mines

SUMMARY

We present a 2D inversion methodology for transversely isotropic media with a tilted symmetry axis (TTI) based on combining reflection moveout with borehole information. The input data include P-wave normal-moveout (NMO) velocities, zero-offset traveltimes and reflection time slopes, as well as vertical group velocities and reflector depths and dips measured in a borehole. For a dipping TTI layer with the symmetry axis confined to the dip plane of the reflector, estimation of the symmetry-direction velocity V_{P0}, the anisotropy parameters ε and δ, and the tilt ν of the symmetry axis proves to be ambiguous despite the borehole constraints. If the symmetry axis is orthogonal to the reflector (a model typical for dipping shale layers), V_{P0} and δ can be recovered with high accuracy, even when the symmetry axis deviates by $\pm 5^\circ$ from the reflector normal. The parameter ε, however, cannot be constrained for dips smaller than 60° without using nonhyperbolic moveout. To invert for the interval parameters of layered TTI media, we apply 2D stacking-velocity tomography supplemented with the same borehole constraints. If the symmetry axis is orthogonal to the reflector in each layer, estimation of the interval parameters V_{P0} and δ remains stable in the presence of Gaussian noise in the input data. Our algorithm can be used to build an accurate initial TTI model for migration velocity analysis.

INTRODUCTION

Tilted TI models play an increasingly important role in seismic processing. In particular, dipping TTI shale layers cause serious imaging problems near salt domes and in fold-and-thrust belts such as the Canadian Foothills (Isaac and Lawton, 1999; Vestrum et al., 1999; Charles et al., 2008; Huang et al., 2008; Behera and Tsvankin, 2009). Also, the symmetry axis is tilted in progradational clastic or carbonate sequences and in the presence of obliquely dipping fractures (Dewangan and Tsvankin, 2006a).

We describe P-wave kinematics in TTI media by the symmetry-direction velocity V_{P0} and the Thomsen (1986) parameters ε and δ defined with respect to the symmetry axis. The symmetry-axis direction in 2D models is determined by the tilt angle ν with the vertical. To resolve the parameters V_{P0}, ε, δ, and ν, which are needed for depth imaging in TTI media, P-wave moveout typically has to be combined with PS- or SS-waves (Grechka and Tsvankin, 2000; Grechka et al., 2002a; Dewangan and Tsvankin, 2006a,b). However, inversion of multicomponent data for the TTI parameters is ambiguous for small and moderate reflector dips and tilts ν (Grechka and Tsvankin, 2000; Grechka et al., 2002a). Also, PS-waves are not always available and their processing is much more involved than that of pure PP reflections.

Here, we include borehole constraints in P-wave stacking-velocity tomography for a model composed of dipping TTI layers and show that stable inversion requires knowledge of the symmetry-axis orientation. Synthetic tests with a realistic level of Gaussian noise illustrate the feasibility of estimating the interval parameters V_{P0}, ε, and δ for a wide range of reflector dips.

INVERSION FOR A SINGLE TTI LAYER

We start by considering the simple model of a homogeneous TTI layer above a planar dipping reflector. To make the problem 2D, the symmetry axis is assumed to be confined to the dip plane. P-wave surface data provide the NMO velocity V_{nmo}, the zero-offset reflection time t_0, and the reflection slope (horizontal slowness) p on the zero-offset time section. At a location where a vertical well is available, one can measure the P-wave vertical group velocity V_{Gw} along with the depth z_w and dip ϕ_w of the reflector (the subscript "w" denotes well data).

The inversion is based on exact expressions for the phase, group, and NMO velocities in homogeneous TI media. Although the input data allow us to construct enough equations for the symmetry-direction velocity V_{P0}, anisotropy parameters ε and δ, and the tilt ν of the symmetry axis, synthetic tests on noise-contaminated data prove the inversion procedure to be highly unstable. This instability is partially caused by the nonlinear dependence of the phase velocity V on the tilt ν (Grechka et al., 2002a).

Symmetry axis orthogonal to the reflector

To overcome the problem caused by an unknown tilt ν, we fixed the symmetry axis in the direction orthogonal to the reflector (Grechka et al., 2002a; Zhou et al., 2008; Behera and Tsvankin, 2009). This common assumption was shown to be adequate for TTI symmetry associated with dipping shale layers (Isaac and Lawton, 1999; Vestrum et al., 1999; Charles et al., 2008).

Inversion methodology

If the symmetry axis coincides with the reflector normal, the tilt ν is equal to the reflector dip ϕ_w measured in the well (Figure 1). Also, the phase-velocity vector of the zero-offset reflection is parallel to the symmetry axis, and the velocity V_{P0} can be obtained directly from surface data and the dip ϕ_w:

$$V_{P0} = \frac{\sin\phi_w}{p} \, . \tag{1}$$

The NMO velocity for $\nu = \phi_w$ is given by the isotropic cosine-of-dip relationship (Tsvankin, 2005):

$$V_{\text{nmo}}(\phi_w) = \frac{V_{\text{nmo}}(0)}{\cos\phi_w} \, , \tag{2}$$

where $V_{\text{nmo}}(0) = V_{P0}\sqrt{1+2\delta}$. Since V_{P0} is already known, equation 2 constrains the parameter δ.

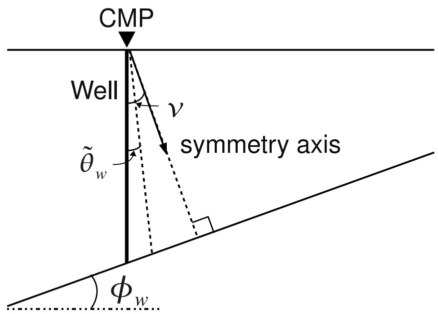

Figure 1: Dipping TTI layer with the CMP at the head of a vertical well. The arrow marks the symmetry axis which is orthogonal to the reflector with the dip ϕ_w. The phase-velocity vector of the vertical ray makes the angle $\tilde{\theta}_w$ with the vertical.

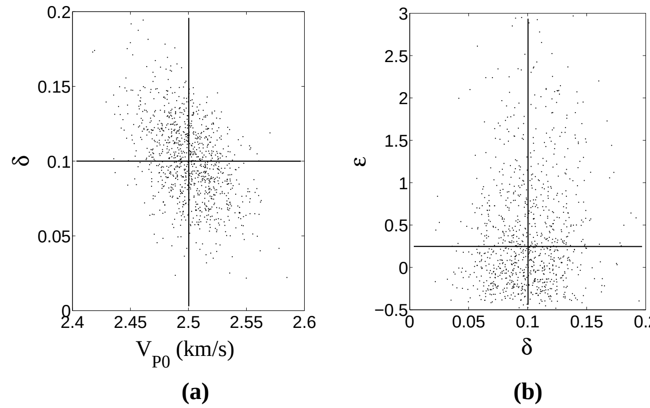

Figure 2: Inverted parameters (dots) for a TTI layer with the symmetry axis orthogonal to its bottom; the dip is 30°. The actual parameter values ($V_{P0} = 2.5$ km/s, $\delta = 0.10$, and $\varepsilon = 0.25$) are marked by the crosses. Due to the large standard deviation (1.37) of ε, the ε-axis on plot (b) is clipped.

The P-wave group velocity V_G in TI media can be obtained from the phase velocity V and the phase angle θ with the symmetry axis (e.g., Tsvankin, 2005):

$$V_G = V \sqrt{1 + \left(\frac{1}{V} \frac{dV}{d\theta} \right)^2}\,, \tag{3}$$

where V depends on the parameters V_{P0}, ε, δ, and θ (θ is taken positive for counter-clockwise rotation from the symmetry axis). We can represent θ through the phase angle $\tilde{\theta}$ with the vertical as $\theta = \tilde{\theta} - \nu$. Then V_G becomes a function of the parameters V_{P0}, ε, δ, $\tilde{\theta}$, and ν:

$$V_G = f_1(V_{P0}, \varepsilon, \delta, \tilde{\theta}, \nu)\,. \tag{4}$$

The P-wave group angle ψ with the symmetry axis is given by (e.g., Tsvankin, 2005):

$$\tan\psi = \frac{\tan\theta + \frac{1}{V}\frac{dV}{d\theta}}{1 - \frac{\tan\theta}{V}\frac{dV}{d\theta}}\,. \tag{5}$$

Therefore, similarly to the group velocity, the group angle $\tilde{\psi}$ with the vertical can be written as

$$\tilde{\psi} = f_2(V_{P0}, \varepsilon, \delta, \tilde{\theta}, \nu)\,. \tag{6}$$

For the P-wave propagating along the well, the group angle with the vertical is zero, but the corresponding phase angle $\tilde{\theta}_w$ is unknown (Figure 1). Applying equations 4 and 6 to the vertical ray yields:

$$f_1(V_{P0}, \varepsilon, \delta, \tilde{\theta}_w, \phi_w) = V_{Gw}\,; \tag{7}$$

$$f_2(V_{P0}, \varepsilon, \delta, \tilde{\theta}_w, \phi_w) = 0\,. \tag{8}$$

Since V_{P0} and δ are already constrained by the zero-offset reflection, the inverse problem reduces to estimating the parameters ε and $\tilde{\theta}_w$ from the vertical group velocity (equations 7 and 8). When $\nu = \phi_w$, the inversion equations do not include z_w and are independent of the CMP location.

Synthetic examples

Figure 2a shows the inversion results for a TTI layer with $\nu = \phi_w = 30°$ and typical values of the Thomsen parameters. We generated 1000 realizations of the input data contaminated by Gaussian noise with the standard deviations equal to 1% for the reflection slope p and 2% for $V_{\rm nmo}$ and V_{Gw}; the starting model was isotropic. As expected from the above analysis, V_{P0} and δ are estimated with high accuracy. Their mean values coincide with the actual parameters ($V_{P0} = 2.50$ km/s, $\delta = 0.1$), and the standard deviations are 1% for V_{P0} and 0.03 for δ. The parameter ε, however, is practically unconstrained (the standard deviation is 1.37; Figure 2b). The instability in estimating ε can be explained using the linearized weak-anisotropy approximation. For weak anisotropy, the phase and group velocities coincide (Thomsen, 1986), and for the vertical ray

$$V_{Gw} = V_{P0}(1 + \delta \sin^2\phi_w \cos^2\phi_w + \varepsilon \sin^4\phi_w)\,. \tag{9}$$

For moderate dips, such as $\phi_w = 30°$ used in the test, the contribution of ε is much smaller than that of δ because ε is multiplied with $\sin^4\phi_w$.

Similar results were obtained for a wide range of small and moderates dips (Table 1). While the inversion produces close estimates of V_{P0} and δ with small (and practically constant) standard deviations, the errors in ε are much larger. To resolve ε from the vertical group velocity, the dip (and tilt) should reach at least 60°. Our algorithm operates with NMO velocity, which controls reflection moveout for offset-to-depth ratios limited by unity. If long-spread P-wave data (with the offset-to-depth ratio reaching two) are available, it is possible to obtain ε from nonhyperbolic moveout (Behera and Tsvankin, 2009).

If the symmetry axis is not orthogonal to the reflector, the algorithm based on setting $\nu = \phi_w$ produces errors in the inverted parameters. However, for typical moderate magnitudes of ε and δ ($|\varepsilon| \le 0.5$; $|\delta| \le 0.3$), the errors in V_{P0} and δ remain small, if the symmetry axis deviates from the reflector normal by less than 5° and the dip ranges from 5° to 50° (Table 2). For example, we computed the input data with the actual tilt $\nu = 15°$ and dip $\phi_w = 20°$, then obtained the param-

Dip (°)	V_{P0} (km/s)		δ		ε	
	sd (%)	mean	sd	mean	sd	mean
5	1	2.50	0.03	0.10	1724	251
10	1	2.50	0.03	0.10	854	282
20	1	2.50	0.03	0.10	48	14.6
30	1	2.50	0.03	0.10	1.37	0.64
40	1	2.50	0.03	0.10	0.29	0.31
50	1	2.50	0.03	0.10	0.13	0.27
60	1	2.50	0.03	0.10	0.07	0.26
70	1	2.50	0.03	0.10	0.05	0.25

Table 1: Inversion results for a single TTI layer with the symmetry axis perpendicular to its bottom. The medium parameters are $V_{P0} = 2.5$ km/s, $\delta = 0.10$, and $\varepsilon = 0.25$. The data were contaminated by Gaussian noise with the standard deviations equal to 1% for p, and 2% for $V_{\rm nmo}$ and V_{Gw}. The standard deviations and mean values of the inverted parameters are denoted by "sd" and "mean", respectively.

Dip (°)	ν (°)	V_{P0} (km/s)		δ	
		sd (%)	mean	sd	mean
5	0	1	2.51	0.03	0.11
5	10	1	2.51	0.03	0.10
20	15	1	2.50	0.03	0.11
20	25	1	2.50	0.03	0.10
40	35	1	2.50	0.03	0.12
40	45	1	2.50	0.03	0.09
60	55	1	2.50	0.03	0.15
60	65	1	2.50	0.03	0.07

Table 2: Inversion results for a TTI layer with the symmetry axis deviating from the reflector normal by $\pm 5°$. The parameters V_{P0} and δ are obtained under the assumption that the symmetry axis is orthogonal to the reflector. The data were contaminated by Gaussian noise with the standard deviations equal to 1% for p, and 2% for $V_{\rm nmo}$ and V_{Gw}.

eters $V_{P0} = 2.5$ km/s and $\delta = 0.11$ under the assumption that $\nu = \phi_w = 20°$. The inversion results become more distorted for strong anisotropy because the value of $\sin\phi_w/p$ differs more significantly from the actual symmetry-direction velocity V_{P0}.

TOMOGRAPHIC INVERSION FOR LAYERED TTI MEDIA

Next, we present a tomographic algorithm for interval parameter estimation in layered TTI media using reflection and borehole data. The model is composed of homogeneous TTI layers separated by planar dipping boundaries with the same azimuth of the dip plane. The symmetry axis in each layer is perpendicular to its bottom, which makes wave propagation 2D. The model vector for an N-layered medium can be written as

$$\widetilde{m} = \{V_{P0}^{(n)}, \varepsilon^{(n)}, \delta^{(n)}, \nu^{(n)}\}, \quad (n = 1, 2, \dots, N). \tag{10}$$

The data vector takes the form

$$\widetilde{d} = \{t_0(n), p(n), V_{\rm nmo}(n), z_w^{(n)}, \phi_w^{(n)}, V_{Gw}^{(n)}\}, \quad (n = 1, 2, \dots, N), \tag{11}$$

where $t_0(n)$, $p(n)$, and $V_{\rm nmo}(n)$ are the effective values for the n-th reflector measured from reflection data, $z_w^{(n)}$ and $\phi_w^{(n)}$ are the depth and dip of the n-th reflector at the well location, and $V_{Gw}^{(n)}$ is the interval vertical group velocity in the n-th layer.

Inversion methodology

The algorithm generalizes the inversion scheme for a single TTI layer discussed above, and represents a modification of stacking-velocity tomography introduced for VTI media by Grechka et al. (2002b). Since the tilt $\nu^{(n)}$ of the symmetry axis in each layer is equal to the dip $\phi_w^{(n)}$, there is a total of $3N$ unknown parameters $\{V_{P0}^{(n)},\ \varepsilon^{(n)},\ \delta^{(n)}\}$ for an N-layered TTI medium.

The model geometry can be fully reconstructed from the known depths and dips of the interfaces. For a given set of the trial interval parameters $\{V_{P0}^{(n)},\ \varepsilon^{(n)},\ \delta^{(n)}\}$, we compute the NMO velocities $V_{\rm nmo,calc}(n)$ using the Dix-type averaging procedure based on tracing the zero-offset ray (Grechka et al., 2002b). Reflection slopes in layered media cannot yield the interval symmetry-direction velocities directly (as in equation 1). Instead, we use the slopes $p(n)$ and zero-offset traveltimes $t_0(n)$ to construct one-way zero-offset rays for the trial TTI parameters and compute the "trial" reflector depths $z_{w,\rm calc}^{(n)}$ in the well. The interval vertical group velocities $V_{Gw,\rm calc}^{(n)}$ are also obtained by ray tracing in the trial model. Fitting the interval velocity $V_{Gw}^{(n)}$ is equivalent to solving equations 7 and 8 for a single layer because the phase angle $\tilde{\theta}_w$ for the vertical ray is obtained from the trial medium parameters.

The interval parameters $\{V_{P0}^{(n)}, \varepsilon^{(n)}, \delta^{(n)}\}$ are estimated by minimizing the objective function that contains the differences between the calculated ("calc") and measured quantities:

$$\mathscr{F}(\widetilde{m}) \equiv \sum_{n=1}^{N} \Big(\big\| V_{\rm nmo,calc}(n) - V_{\rm nmo}(n) \big\| + \big\| z_{w,\rm calc}^{(n)} - z_w^{(n)} \big\| + \big\| V_{Gw,\rm calc}^{(n)} - V_{Gw}^{(n)} \big\| \Big). \tag{12}$$

The dips $\phi_w^{(n)}$ are not included in the objective function because they are used to constrain the tilt $\nu^{(n)}$ of the symmetry axis in each layer. For a single layer, the parameter ε is obtained from the vertical velocity (equations 7 and 8). However, for layered TTI media, $\varepsilon^{(n)}$ also contributes to $V_{\rm nmo,calc}(n)$ (except for $n = 1$) and $z_{\rm calc}^{(n)}$. Therefore, $\varepsilon^{(n)}$ has to be estimated together with $V_{P0}^{(n)}$ and $\delta^{(n)}$ from equation 12. This tomographic algorithm can be applied to a single CMP since each layer is laterally homogeneous with planar boundaries.

It should be emphasized that we invert for all interval parameters simultaneously without employing layer stripping. This feature of the algorithm helps to reduce error accumulation with depth and is particularly beneficial when the model includes a layer at depth that is known to be isotropic. Then, as demonstrated by Grechka et al. (2001) on physical-modeling

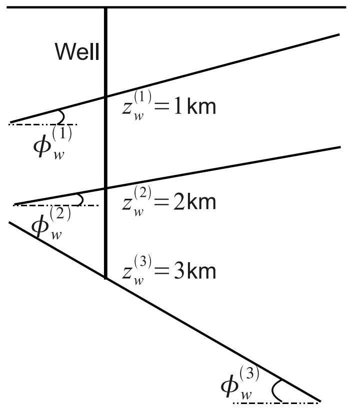

Figure 3: Three-layer TTI model used to test the tomographic algorithm. The dips are $\phi_w^{(1)} = 15°$, $\phi_w^{(2)} = 10°$, and $\phi_w^{(3)} = -30°$. The reflector depths at the well location are $z_w^{(1)} = 1$ km, $z_w^{(2)} = 2$ km, and $z_w^{(3)} = 3$ km.

data for a bending TTI thrust sheet, the reflection from the bottom of the isotropic layer provides valuable constraints on the parameters of the TTI overburden.

Synthetic example

The algorithm was tested on a three-layer TTI model with dipping interfaces (Figure 3) and the interval parameters listed in Table 3. The inversion results for 200 realizations of noise-contaminated input data are shown in Figure 4. Since the dips are moderate, estimation of the interval parameter ε is highly unstable, while V_{P0} and δ are well constrained. The standard deviations in the inverted parameters are higher in the third layer (about 2% for V_{P0}, and 0.04 for δ). This reduction in accuracy is due primarily to the smaller contribution of the deeper layers to the effective reflection traveltimes. As was the case for a single layer, rotating the symmetry axis by $\pm 5°$ from the reflector normal does not substantially distort the estimates of V_{P0} and δ.

	Layer 1	Layer 2	Layer 3
V_{P0} (km/s)	1.5	2.0	2.5
ε	0.10	0.50	0.25
δ	-0.10	0.30	0.10
ν (°)	15	10	-30

Table 3: Interval parameters of the three-layer TTI model from Figure 3. The symmetry axis in each layer is orthogonal to its lower boundary. The input data were distorted by Gaussian noise with the standard deviations equal to 1% for $t_0(n)$ and $p(n)$ and 2% for $V_{\rm nmo}$ and V_{Gw}.

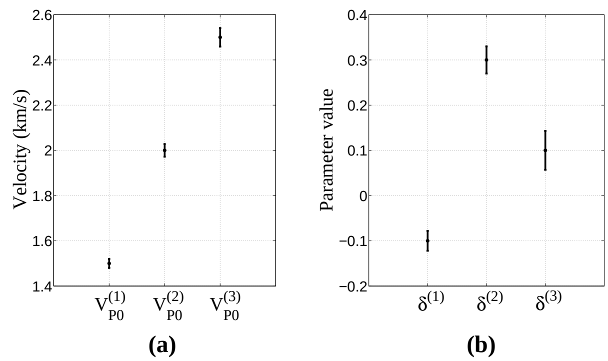

Figure 4: Interval symmetry-direction velocities $V_{P0}^{(n)}$ (a) and the anisotropy parameters $\delta^{(n)}$ (b) estimated by the tomographic inversion for the three-layer model from Figure 3 and Table 3. The dots mark the exact values, and the bars correspond to the $\pm$ standard deviation in each parameter.

CONCLUSIONS

We devised a parameter-estimation algorithm for tilted transverse isotropy that operates with conventional-spread P-wave moveout and borehole data. The semi-analytic inversion procedure for a single TTI layer showed that the parameters V_{P0}, ε, and δ cannot be resolved without assuming the symmetry axis to be orthogonal to the reflector. To estimate the interval parameters of a stack of TTI layers separated by plane dipping interfaces, we employed stacking-velocity tomography combined with vertical group velocities and reflector depths and dips measured in a borehole. The current implementation is limited to 2D models, in which the vertical incidence plane coincides with the dip plane in each layer. By performing the inversion for all layers simultaneously, the algorithm mitigates error accumulation with depth and produces more stable results for TTI formations overlying isotropic strata. Tests on noise-contaminated data demonstrate that the interval parameters V_{P0} and δ are well constrained for a wide range of reflector dips, while the inversion for ε requires the dip to reach at least 60°. The method can be extended in a straightforward way to 3D wide-azimuth P-wave data by replacing the NMO velocities in the objective function with the NMO ellipses.

Stacking-velocity tomography, possibly combined with non-hyperbolic moveout inversion for ε, represents an efficient tool for building an initial model for migration velocity analysis and post-migration reflection tomography. After carrying out the interval parameter estimation at well locations, the V_{P0}- and δ-fields can be computed by interpolation between the wells.

ACKNOWLEDGMENTS

We are grateful to Andrey Bakulin and Paul Fowler (both of WesternGeco), Vladimir Grechka (Shell), and Andres Pech (IPN, Mexico) for making available their codes and numerous helpful suggestions. We are also grateful to our colleagues from the Center for Wave Phenomena (CWP) for valuable discussions and technical help. This work was supported by the Consortium Project on Seismic Inverse Methods for Complex Structures at CWP.

REFERENCES

Behera, L. and I. Tsvankin, 2009, Migration velocity analysis for tilted TI media: Geophysical Prospecting, **57**, 13–26.

Charles, S., D. R. Mitchell, R. A. Holt, J. Lin, and J. Mathewson, 2008, Data-driven tomographic velocity analysis in tilted transversely isotropic media: A 3D case history from the Canadian Foothills: Geophysics, **73**, VE261–VE268.

Dewangan, P. and I. Tsvankin, 2006a, Modeling and inversion of PS-wave moveout asymmetry for tilted TI media: Part I – Horizontal TTI layer: Geophysics, **71**, D107–D121.

———, 2006b, Modeling and inversion of PS-wave moveout asymmetry for tilted TI media: Part II – Dipping TTI layer: Geophysics, **71**, D123–D134.

Grechka, V., A. Pech, and I. Tsvankin, 2002a, Multicomponent stacking-velocity tomography for transversely isotropic media: Geophysics, **67**, 1564–1574.

———, 2002b, P-wave stacking-velocity tomography for VTI media: Geophys. Prosp., **50**, 151–168.

Grechka, V., A. Pech, I. Tsvankin, and B. Han, 2001, Velocity analysis for tilted transversely isotropic media: A physical-modeling example: Geophysics, **66**, 904–910.

Grechka, V. and I. Tsvankin, 2000, Inversion of azimuthally dependent NMO velocity in transversely isotropic media with a tilted axis of symmetry: Geophysics, **65**, 232–246.

Huang, T., S. Xu, J. Wang, G. Ionescu, and M. Richardson, 2008, The benefit of TTI tomography for dual azimuth data in Gulf of Mexico: SEG Expanded Abstracts, **27**, 222–226.

Isaac, J. H. and D. C. Lawton, 1999, Image mispositioning due to dipping TI media: A physical seismic modeling study: Geophysics, **64**, 1230–1238.

Thomsen, L., 1986, Weak elastic anisotropy: Geophysics, **51**, 1954–1966.

Tsvankin, I., 2005, Seismic signatures and analysis of reflection data in anisotropic media, 2nd edition: Elsevier Science Publ. Co., Inc.

Vestrum, R., D. C. Lawton, and R. Schmid, 1999, Imaging structures below dipping TI media: Geophysics, **64**, 1239–1246.

Zhou, B., S. Greenhalgh, and A. Green, 2008, Nonlinear traveltime inversion scheme for crosshole seismic tomography in titled transversely isotropic media: Geophysics, **73**, D17–D33.